

fig1_eddy-feedback-parameter_calculation_steps.png.

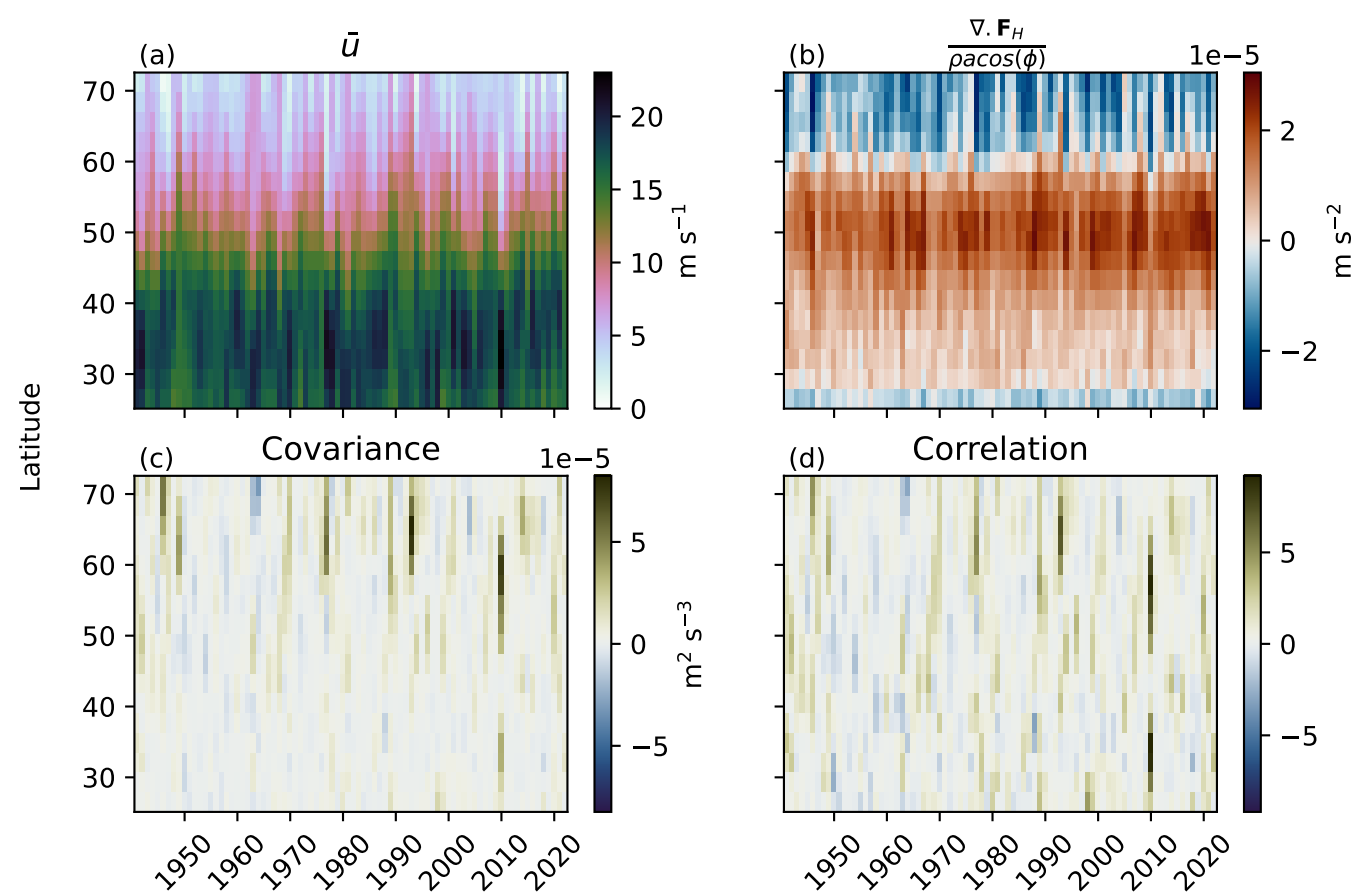
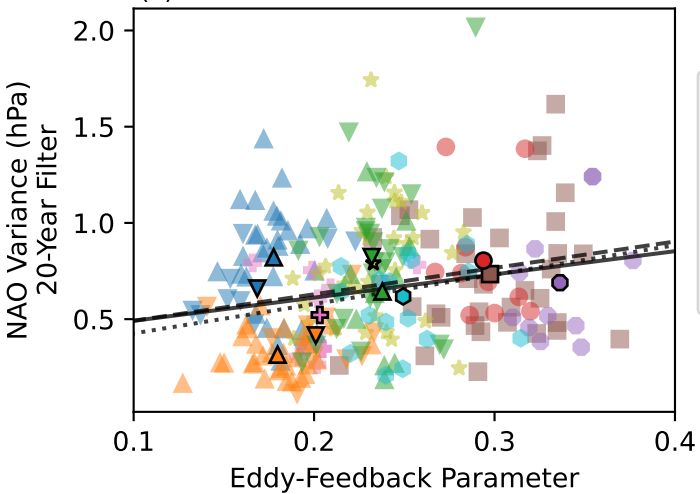
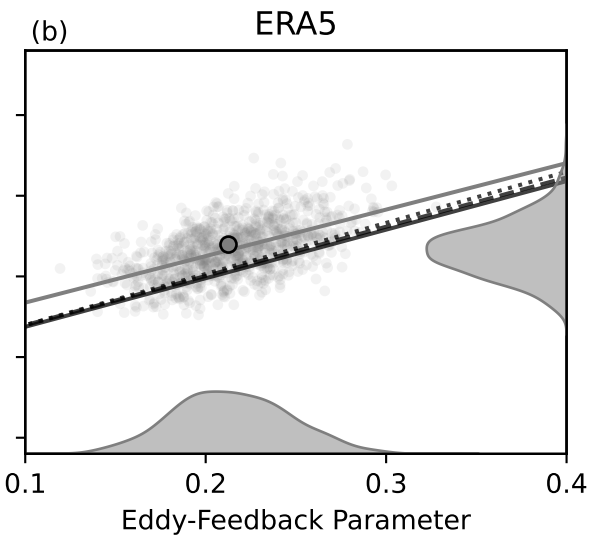
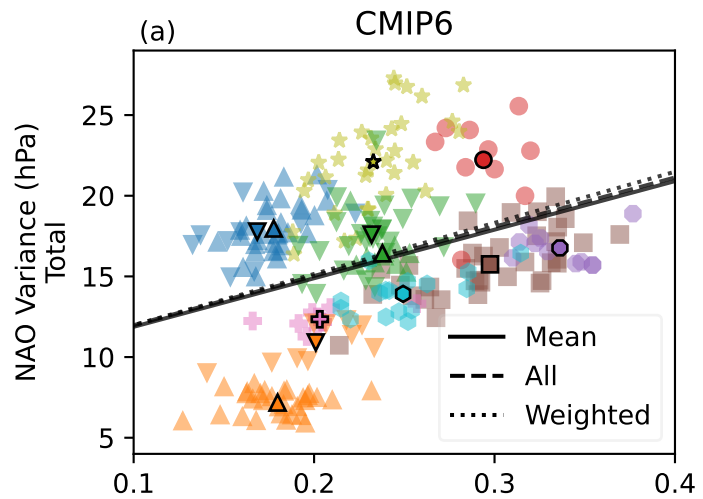


fig3_efp_nao_correlation_cmip6_DJF_1850-2014.png.

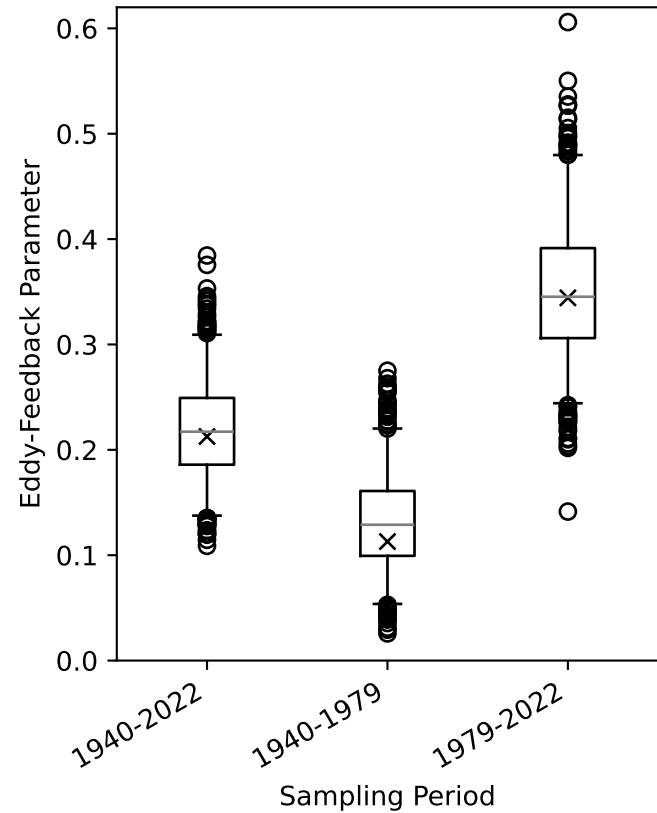


- | | |
|----------------|-----------------|
| ● CESM2 | ★ IPSL-CM6A-LR |
| ● CMCC-CM2-SR5 | ▲ MIROC-ES2L |
| ▲ CNRM-CM6-1 | ▼ MIROC6 |
| ▼ CNRM-ESM2-1 | ▲ MPI-ESM1-2-HR |
| ■ CanESM5 | ▼ MPI-ESM1-2-LR |
| ✖ INM-CM5-0 | ◆ UKESM1-0-LL |

fig2_efp_reanalysis_uncertainties.png.

Eddy-Feedback Parameter - Reanalysis Uncertainties

(a) Sampling Uncertainty



(b) Multidecadal Variability

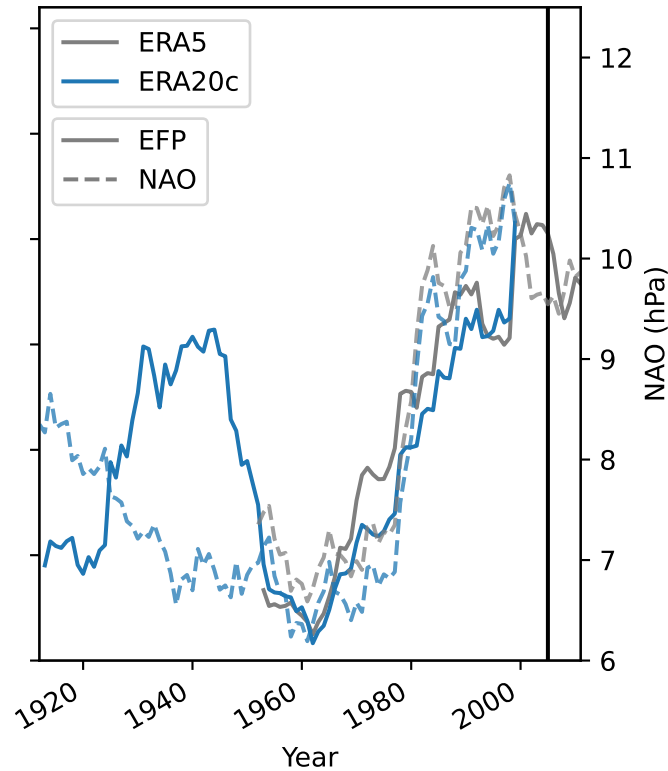
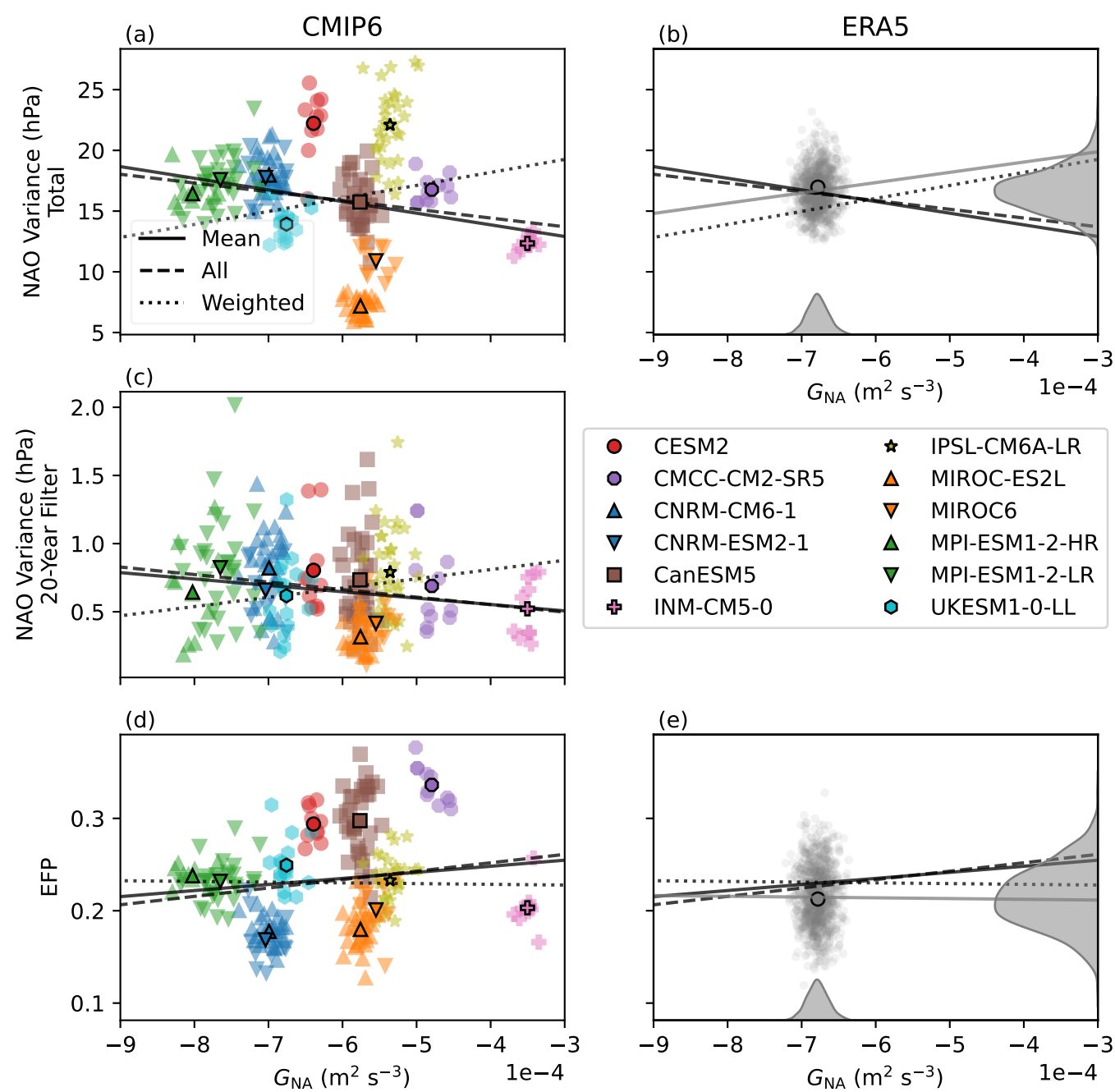


fig4_lefp-in-box-cmip6_vs_efp_and_nao.png.



1 **Large sampling uncertainty when diagnosing the ‘eddy
2 feedback parameter’ and its role in the signal-to-noise
3 paradox**

4 **Leo Saffin^{1,2}, Christine M. McKenna^{1,3}, Rémy Bonnet⁴, and Amanda C.
5 Maycock¹**

6 ¹School of Earth and Environment, University of Leeds, Leeds, UK

7 ²Department of Meteorology, University of Reading, Reading, UK

8 ³JBA Consulting, Warrington, UK

9 ⁴CECI, Université de Toulouse, CERFACS/CNRS, Toulouse, France

10 **Key Points:**

- 11 • The ‘eddy feedback parameter’ is a highly non-stationary quantity, making reanal-
12 ysis and model comparisons problematic on short time periods
- 13 • Sampling uncertainty in the eddy feedback parameter from reanalysis data is com-
14 parable to the intermodel spread across models
- 15 • Barotropic energy generation rate is a more stable quantity, but does not explain
16 model spread in North Atlantic climate variability

17 **Abstract**

18 Model forecasts on seasonal-to-decadal timescales have recently been shown to have
 19 significant skill in predicting the North Atlantic Oscillation (NAO, a large-scale pattern
 20 of variability). However, these forecasts are undermined by signal-to-noise ratios that
 21 are lower than expected given the skill, meaning the models are underconfident. This
 22 problem is known as the “signal-to-noise paradox”. Previous work has shown that mod-
 23 els underestimate the strength of feedback from atmospheric eddies onto the midlatitude
 24 circulation, but models with a stronger eddy feedback suffer less from the signal-to-noise
 25 paradox. However, we find that the “eddy feedback parameter” (EFP) used in these stud-
 26 ies exhibits large sampling uncertainty that has not previously been taken into account.
 27 When accounting for this sampling uncertainty, the EFP in models is generally consist-
 28 ent with reanalysis data. Furthermore, across samples, the EFP correlates with the vari-
 29 ability of the NAO, meaning they are not independent, which makes the EFP problem-
 30 atic for understanding the causes of the signal-to-noise paradox. Samples with larger NAO
 31 variability are diagnosed with a larger EFP, even within the same dataset. An alterna-
 32 tive measure of eddy feedback is less sensitive to sampling and better identifies models
 33 which have weak, strong, or unbiased eddy feedbacks.

34 **Plain Language Summary**

35 Model forecasts on seasonal-to-decadal timescales have recently been shown to have
 36 significant skill in predicting the North Atlantic Oscillation (NAO, a large-scale pattern
 37 of variability). However, these forecasts are undermined by signal-to-noise ratios that
 38 are lower than expected given the skill, meaning the models are underconfident and larger
 39 ensembles of simulations are needed to be able to extract the predictable signal. This
 40 problem is known as the “signal-to-noise paradox”. Previous work has shown that mod-
 41 els tend to underestimate the strength of feedback from atmospheric eddies onto the mid-
 42 latitude circulation, but models with a stronger eddy feedback suffer less from the signal-
 43 to-noise paradox, suggesting that more confident predictions would be possible if eddy
 44 feedbacks in models were improved. However, we find that the “eddy feedback param-
 45 eter” (EFP) used in these studies exhibits large sampling uncertainty that has not pre-
 46 viously been taken into account. When accounting for this sampling uncertainty, the EFP
 47 in models is generally consistent with reanalysis data, rather than being too weak. Fur-
 48 thermore, across samples, the EFP correlates with the variability of the NAO, meaning
 49 they are not independent. The lack of independence between the EFP and the NAO makes
 50 the EFP problematic for understanding the causes of the signal-to-noise paradox. What
 51 could have been interpreted as models with a stronger eddy feedback giving stronger NAO
 52 variability, is actually a result of samples with larger NAO variability being diagnosed
 53 with a larger EFP, even within the same dataset. We test an alternative measure of eddy
 54 feedback and find it is much less sensitive to sampling issues than the EFP, finding no
 55 systematic model bias but better distinguishing which models have weak, strong, or un-
 56 biased eddy feedbacks.

57 **1 Introduction**

58 The winter North Atlantic Oscillation (NAO) has been shown to be predictable on
 59 seasonal (Scaife et al., 2014) and decadal (Smith et al., 2019) timescales. However, the
 60 predictable NAO signal in models (variability of the ensemble mean) is weaker than ex-
 61 pected given the skill, meaning forecasts are underconfident (Scaife & Smith, 2018). This
 62 underconfidence occurs despite models having a relatively good representation of total
 63 NAO variability and has been coined the signal-to-noise paradox (Scaife et al., 2014; Scaife
 64 & Smith, 2018). This underconfidence could be a manifestation of a too-large compo-
 65 nent of forecast noise or a too-weak predictable signal (Eade et al., 2014; Scaife & Smith,
 66 2018).

Several studies have investigated whether predictable NAO signals are poorly captured in models, including the representation of teleconnections from the tropics to the North Atlantic (O'Reilly et al., 2019; Williams et al., 2023), the response to Arctic sea ice anomalies (Smith et al., 2022), the response to North Atlantic sea surface temperature (SST) anomalies (Simpson et al., 2018), the response to solar cycle variability (Gray et al., 2013; Scaife et al., 2014) and the response to predictable tropical stratospheric variability (Andrews et al., 2019).

There are currently two main hypotheses to explain the NAO signal-to-noise problem.

1. Weak air-sea coupling in the North Atlantic. This has been shown to contribute to an underestimation of winter North Atlantic eddy-driven jet variability on multidecadal timescales (Simpson et al., 2018; Bracegirdle et al., 2018) and summer NAO variability on decadal timescales (Ossó et al., 2020).
2. Weak eddy feedbacks in midlatitudes. Eddy momentum fluxes can act to reinforce the zonal-mean flow and increase the persistence of jets (Lorenz & Hartmann, 2001, 2003) and the NAO is known to be driven by momentum forcing from synoptic and stationary eddies (Luo et al., 2007). Smith et al. (2022) introduced the “eddy feedback parameter” (EFP) to quantify the relationship between eddy forcing and the midlatitude jet (see Section 2.2.1). Smith et al. (2022) showed the EFP in present day climate correlated with the amplitude of the midlatitude zonal wind response to projected Arctic sea ice loss across a set of climate models. They showed that models underestimated the EFP compared to reanalyses and used an emergent constraint approach to derive a constrained spread of the modeled jet shift. Hardiman et al. (2022) found that models with a weaker EFP (further from reanalysis) generally have less skill and worse signal-to-noise errors for predicting the Northern hemisphere winter circulation.

Most of the work on the NAO signal-to-noise problem has focused on seasonal-to-decadal timescales; it remains an open question as to whether similar issues manifest in multidecadal projections of the NAO including externally forced trends (McKenna & Maycock, 2021). The initial motivation of this work was to test the eddy feedback hypothesis in climate simulations by examining whether the EFP is related to multidecadal NAO variability. However, we found that our results were strongly affected by sampling issues with the EFP not accounted for in past studies. In this study, we address the sampling uncertainty in the EFP within reanalysis and climate model datasets, as well as the inherent relationship between the EFP and NAO characteristics within a sample. The EFP is based on zonal-mean data and does not separate the timescales of eddies and the mean flow. Therefore, we also analyze a spatially-resolved diagnostic of eddy feedback, the barotropic energy generation rate (Mak & Cai, 1989), which allows us to investigate the relationship between North-Atlantic eddy feedback and NAO variability using time-filtered data.

This study is laid out as follows: Section 2 describes the datasets used in the study and methods for quantifying eddy-mean flow feedback, Section 3 presents the results and Section 4 presents a summary of the key findings.

2 Methods

2.1 Datasets

Climate model data is taken from phase 6 of the Coupled Model Intercomparison Project (CMIP6) (Eyring et al., 2016). We use the historical experiment (1850-2014) from 12 CMIP6 models that provide the required variables (monthly-mean mean-sea-level pressure, and daily-mean zonal (u) and meridional (v) wind on pressure levels) for at least 10 ensemble members (see supplement Table S6). We select models that provide large

116 ensembles in order to quantify sampling effects and the role of internal variability in cal-
 117 culating the EFP and its relationship with the NAO. Diagnostics are calculated from data
 118 regridded to the coarsest resolution climate model (CanESM5, roughly 2.8°). All diag-
 119 nóstics are for Northern hemisphere winter (DJF) with the year labeled by the JF (e.g.
 120 2009/10 is labeled 2010).

121 We use the ERA5 (Hersbach et al., 2020) and ERA20C (Poli et al., 2016) reanal-
 122 ysis datasets. The back extension of ERA5 covers the period 1940 to 1978 and the stan-
 123 dard ERA5 covers 1979 to present. ERA20C covers 1900-2010 and only assimilates sur-
 124 face pressure and surface marine wind observations. For ERA5 and ERA20C winds, we
 125 aggregate six hourly data (00, 06, 12, 18) to daily means to provide an equivalent com-
 126 parison to the CMIP6 data. We also use monthly-mean mean-sea-level pressure data from
 127 20CRv3 (Slivinski et al., 2019), a longer timescale reanalysis that only assimilates sur-
 128 face pressure, and HadSLP (Allan & Ansell, 2006), a gridded dataset produced from sur-
 129 face pressure observations, to calculate NAO timeseries in the supplement.

130 2.2 Diagnostics

131 2.2.1 Eddy feedback parameter

132 Smith et al. (2022) defined the eddy feedback parameter (EFP) as the squared cor-
 133 relation coefficient (r^2) between the DJF-mean zonal-mean zonal wind (\bar{u}) and the DJF-
 134 mean of the horizontal component of the Eliassen-Palm flux (EP-flux) divergence, cal-
 135 culated as a function of latitude and pressure, and then averaged over $25\text{-}72^\circ\text{N}$, and 200-
 136 600 hPa. Hardiman et al. (2022) used a similar formulation, but calculated the EFP at
 137 a single level (500 hPa) and only included the quasi-geostrophic component of EP-flux di-
 138 vergence, expressed as a zonal acceleration: eq. 1 from Hardiman et al. (2022),

$$\frac{\nabla \cdot \mathbf{F}_H}{\rho \cos(\phi)} = -\frac{1}{a \cos^2 \phi} \frac{d(\bar{u}' v' \cos^2 \phi)}{d\phi}, \quad (1)$$

139 where ρ is density, ϕ is latitude, a is Earth's radius. Overbars represent a zonal mean,
 140 and primes represent local deviations from the zonal mean. Here, we calculate the EFP
 141 following Hardiman et al. (2022). The differences in methodology for calculating the EFP
 142 can give a different absolute value, but give similar results for the uncertainty (see sup-
 143 plement Fig. S1).

144 2.2.2 Barotropic energy generation rate

145 The barotropic energy generation rate (G) diagnoses the exchange of energy be-
 146 tween eddies and the large-scale flow based on an energy equation for the ageostrophic
 147 perturbation flow in quasi-geostrophic dynamics (Mak & Cai, 1989). If (U, V) describes
 148 the large-scale geostrophic wind and (u', v') the eddies, then the barotropic energy gen-
 149 eration rate is given by

$$G = \mathbf{E} \cdot \mathbf{D}, \quad (2)$$

150 where

$$\mathbf{E} = \cos(\phi) \left(\frac{1}{2}(v'^2 - u'^2), -u'v' \right), \quad (3)$$

151 is the E-vector, which describes the elongation of the eddy, and

$$\mathbf{D} = \frac{1}{a \cos(\phi)} \left(\frac{\partial U}{\partial \lambda} - \frac{\partial V \cos(\phi)}{\partial \phi}, \frac{\partial V}{\partial \lambda} + \frac{\partial U \cos(\phi)}{\partial \phi} \right), \quad (4)$$

152 is the deformation of the large-scale flow (Mak & Cai, 1989), where λ is latitude. Note
 153 that we use the spherical coordinate version of these equations from Fukotomi and Ya-
 154 sunari (2002). We diagnose G using daily-mean winds at 250 hPa that are separated into
 155 a high frequency (2-6 day) eddy component and a slowly varying (> 10 day) large-scale
 156 component using Lanczos filters with a window of 61 days.

157 In comparison to the EFP, G is spatially-resolved, giving a measure of the local en-
 158 ergy exchange. To provide a comparison with the EFP and relate G to NAO variabil-
 159 ity, we average G over a box in the North Atlantic (60° – 25° W, 30° – 45° N) giving G_{NA} .
 160 This region is where the models and reanalysis show climatological negative values (see
 161 supplement Fig. S2), indicating exchange of energy from the eddies to the large scale flow.

162 2.2.3 North Atlantic Oscillation index

163 The NAO index is calculated as the difference in DJF area-averaged mean-sea-level
 164 pressure between a southern box (90° W– 60° E, 20° N– 55° N) and a northern box (90° W– 60° E,
 165 55° N– 90° N) following Stephenson et al. (2006). From the NAO timeseries we calculate
 166 variance. Multidecadal NAO variance is also calculated by first applying a 20-year run-
 167 ning mean.

168 The NAO has not been detrended, which could lead to a overestimation of NAO
 169 variance in the CMIP6 models compared to ERA5 because we are retaining longer-timescale
 170 variability. However, multidecadal variability is only a small part of the total NAO vari-
 171 ance (see section 3.3), so the difference in NAO variance due to including these longer
 172 timescales is small.

173 2.3 Statistics

174 To estimate sampling uncertainty, we recalculate the EFP in ERA5 by resampling
 175 winters with replacement (bootstrapping) using the same sample size as the input dataset
 176 (e.g. for 1940–2022, each sample is 82 years), repeating 1000 times. We also recalculate
 177 the EFP, NAO variance, and G_{NA} in ERA5 in the same way, but with a sample size match-
 178 ing the historical simulation length (164 years) to compare with the CMIP6 simulations.
 179 Each diagnostic is calculated using the same sample years, allowing us to assess relation-
 180 ships between these diagnostics due to sampling. Relationships between variables are es-
 181 timated using linear least squares regression.

182 3 Results

183 3.1 Uncertainties in reanalysis derived eddy feedback parameter

184 In this section, we show how the EFP is affected by sampling uncertainty and mul-
 185 t tidecadal variability. Figure 1 shows the calculation of the EFP in ERA5 broken into con-
 186 stituent steps. Figure 1a and 1b show the DJF-mean input variables as a function of lat-
 187 itude and year: \bar{u} and the acceleration of \bar{u} diagnosed from the quasigeostrophic compo-
 188 nent of the horizontal EP-flux divergence. The EFP is calculated by calculating the cor-
 189 relation coefficient (r) between these two variables at each latitude and then averaging
 190 r^2 across latitudes. r is defined as the covariance of two variables normalized by their
 191 standard deviations. To understand how different years and latitudes contribute to the
 192 EFP, Fig. 1c shows the anomalies of the input variables, relative to the time mean at
 193 each latitude, multiplied together, so the time mean is the covariance as a function of
 194 latitude. Figure 1d shows the same, but normalized by the standard deviations of the
 195 input variables at each latitude, so the time mean is r as a function of latitude.

196 Figure 1 reveals two potential issues with the EFP:

- 197 1. Calculating r at each latitude and then taking a spatial average overemphasizes
 198 latitudes with weaker variability. This can be seen by comparing Fig. 1c and 1d:
 199 anomalies are weaker closer to the equator for the covariance but have a larger con-
 200 tribution to r because the standard deviation at those latitudes is smaller.
- 201 2. A single outlier season can make a large contribution to the EFP (e.g. 2009/2010
 202 in Fig. 1d). This undermines comparisons of the EFP in reanalysis data and cli-

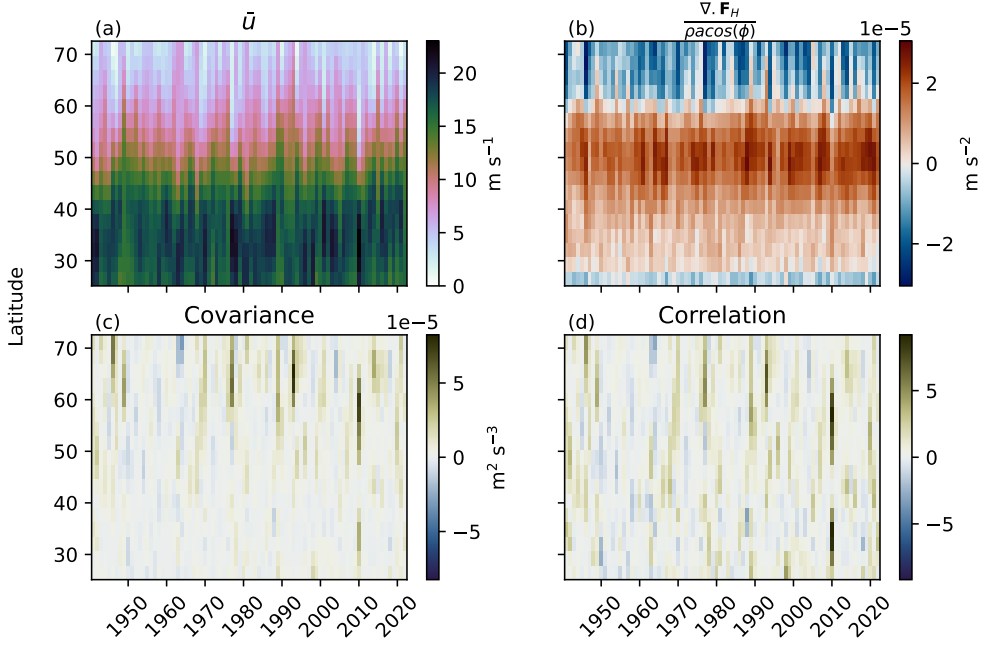


Figure 1. Calculation of the EFP using ERA5. Variables used to calculate the EFP as a DJF mean, (a) zonal-mean zonal wind and (b) the acceleration of the zonal-mean zonal wind diagnosed from the quasi-geostrophic component of the horizontal EP-flux divergence. (c) The product of anomalies of (a) and (b), where the anomalies are calculated against the time mean (mean across rows) by latitude. (d) shows the same as (c), but normalized by the standard deviations, at each latitude, of (a) and (b). The time mean of (c) and (d) give the covariance and correlation as a function of latitude, respectively.

203 estimate models when they do not span a common period and do not sample the same
 204 internal variability. For example, if a model with inherently weak eddy feedback
 205 happens to simulate a season like 2009/2010, it may appear to have a larger EFP
 206 than a model with a strong eddy feedback that by chance does not simulate a sea-
 207 son like 2009/2010.

208 Building on point 2, to quantify the sampling uncertainty we recalculate the EFP
 209 by sampling years from ERA5 with replacement (see Section 2.3). Figure 2a shows re-
 210 sults with the resampling period varied to show the dependence of “observed” EFP on
 211 time period: the full ERA5 period (1940-2022); the pre-satellite backward extension pe-
 212 riod only (1940-1979); and the satellite period only (1979-2022). In all cases, the sam-
 213 pling uncertainty in the EFP ($\approx 0.2\text{-}0.3$) is comparable to the median value based on
 214 the 95% confidence interval. This sampling effect represents a substantial uncertainty
 215 that has not been acknowledged in previous studies (e.g., Smith et al. (2022); Hardiman
 216 et al. (2022); Screen et al. (2022)).

217 Figure 2a also shows the EFP is dependent on time period: the satellite period has
 218 a larger EFP than the pre-satellite back extension period, with no overlap of the 95%
 219 intervals. To better understand the dependence of EFP on time period, we calculate the
 220 EFP using a rolling 23-year window (consistent with the 1993-2016 period used in Hardiman
 221 et al. (2022)). ERA5 shows a systematic increasing trend in the 23-year EFP (Fig. 2b)).
 222 A long-term trend in the EFP could be spurious if the reanalysis is poorly constrained
 223 by observations and behaves more like the underlying atmospheric model further back

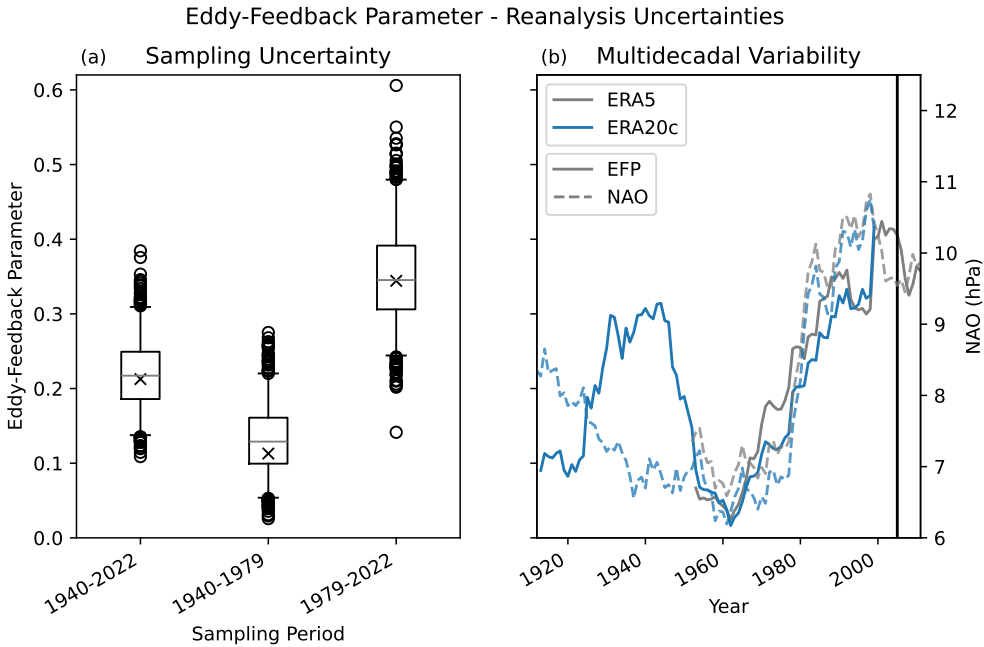


Figure 2. Uncertainties in the EFP identified from reanalysis data. (a) The EFP calculated by resampling ERA5 over different periods. Orange lines show the median, crosses show the EFP from the original set of years, boxes show the 25-75% range, whiskers show the 2.5-97.5% range, and circles show points outside this range. (b) The EFP calculated over 23-year rolling windows and 23-year running mean NAO for ERA5 and ERA20C data. The x-axis shows the middle year in each sample. The vertical line is for 1993-2016, the years used in Hardiman et al. (2022).

in time. Figure 2b also shows the EFP from ERA20C, which extends back to 1900. Longer-term reanalyses that only assimilate a limited set of surface observations, such as ERA20C, have been shown to produce unrealistic trends as the density of the observation network evolves with time (Krueger et al., 2013; Oliver, 2016; Befort et al., 2016; Bloomfield et al., 2018). However, ERA20C actually shows a larger EFP in the 1930s/1940s when there is less observation data and reproduces the increase in EFP over the late 20th century. This shows the apparent EFP trend is unlikely to be due to an intrinsic bias of weak eddy feedback in the model that produces ERA5 and instead is related to multidecadal variability in the input parameters.

Interestingly, the increase in EFP over the late 20th century closely mirrors the positive trend in the NAO over this period, though this common temporal behavior does not appear in the earlier period covered only by ERA20C. It makes sense that the NAO and EFP are related. Eddy-driven jet latitude is related to the NAO (Woollings et al., 2010) and NAO predictability (Parker et al., 2019; Strommen, 2020), and zonal-mean zonal wind is one of the inputs to the EFP calculation. The EFP calculation also emphasizes large seasonal deviations in jet latitude. For example, winter 2009/10 had a strongly southward shifted jet and negative NAO (Santos et al., 2013). Figure 1d showed how the shift in jet in 2009/10 is emphasized in the correlation calculation and Fig. 2b shows a step increase of almost 0.1 when 2009/10 is included in the rolling window.

The time period used by Hardiman et al. (2022) (1993-2016) is very close to the maximum EFP over the entire 20th century due to the inclusion of 2009/10 and the coincidence with a “high phase” of multidecadal variability. The results in this section show

246 that previous studies have likely overestimated the long-term mean EFP in reanalysis
 247 data.

248 249 3.2 Comparison of climate models and reanalysis eddy feedback parameter

250 We next address the comparison of EFP in climate models with reanalysis data in
 251 the context of the sampling uncertainties described in the previous section. Figure 3 shows
 252 the range of EFP calculated from the CMIP6 ensembles (a, c) and from repeatedly sam-
 253 pling 164 years from ERA5 with replacement (b), as well as the relationship with NAO
 254 variance (discussed in the following section). In contrast to previous results, we do not
 255 find that the EFP is weaker in models than in reanalysis. The EFP diagnosed from CMIP6
 256 models is generally within the uncertainty from ERA5, with some models potentially hav-
 257 ing too large EFP (CanESM5, CESM2, CMCC-CM2-SR5). If we only considered the
 258 EFP and its associated uncertainty from the satellite period of ERA5 (Fig. 2a), then we
 259 would conclude that some CMIP6 models underestimate the EFP. This highlights the
 260 importance of considering longer-timescale variability, as well as sampling uncertainty,
 261 when quantifying the EFP and the limitation of using the EFP as a diagnostic for model
 262 performance.

263 264 3.3 Relationship between the eddy feedback parameter and the North Atlantic oscillation

265 Section 3.1 highlighted a relationship between long-term variations in the EFP and
 266 the NAO. We next show how this relationship can lead to correlations that should be
 267 interpreted as a sample with larger NAO variability giving a larger EFP, rather than stronger
 268 eddy feedbacks leading to stronger NAO variability. Most CMIP6 models capture NAO
 269 variability well (Fig. 3a) compared to ERA5 (Fig. 3b). Only MIROC-ES2L is system-
 270 atically too weak. Some models are potentially too weak (MIROC6, INM-CM5-0) or too
 271 strong (IPSL-CM6A-LR, CESM2), but produce ensemble members within the range of
 272 ERA5 uncertainty.

273 The lines in Fig. 3 show linear regressions calculated from the data in each panel
 274 in different ways:

- 275 1. For “ERA5” (gray line in Fig. 3b) the regression is across the bootstrap samples.
 276 Because EFP and NAO variance are calculated using the same sets of sample years,
 277 this tells us how the EFP relates to NAO variability purely due to sampling.
- 278 2. “Mean” is the regression across the ensemble mean points of all models. This re-
 279 lates to model biases and is what would typically be used for emergent constraints
 280 (e.g. Smith et al. (2022))
- 281 3. “Weighted” is a weighted average regression across all models. For each model,
 282 a regression is calculated across ensemble members. The average slope and inter-
 283 cept are then calculated from these individual model regressions, weighted by the
 284 number of ensemble members for each model. This indicates whether a sampling
 285 relationship between EFP and NAO variability is present, on average, in individ-
 286 ual models.
- 287 4. “All” is the regression across all ensemble members of all models with each sam-
 288 ple treated independently. This gives a mix between “Mean” and “Weighted”.

289 The full set of results from the linear regressions are given in the supplement (Tables S1-
 290 S5). Note that many of the individual model regressions in 3) are not significant due to
 291 low sample sizes and the p-value test is less meaningful for the “ERA5” and “All” re-
 292 gressions because the points are not independent. However, the analysis is intended to

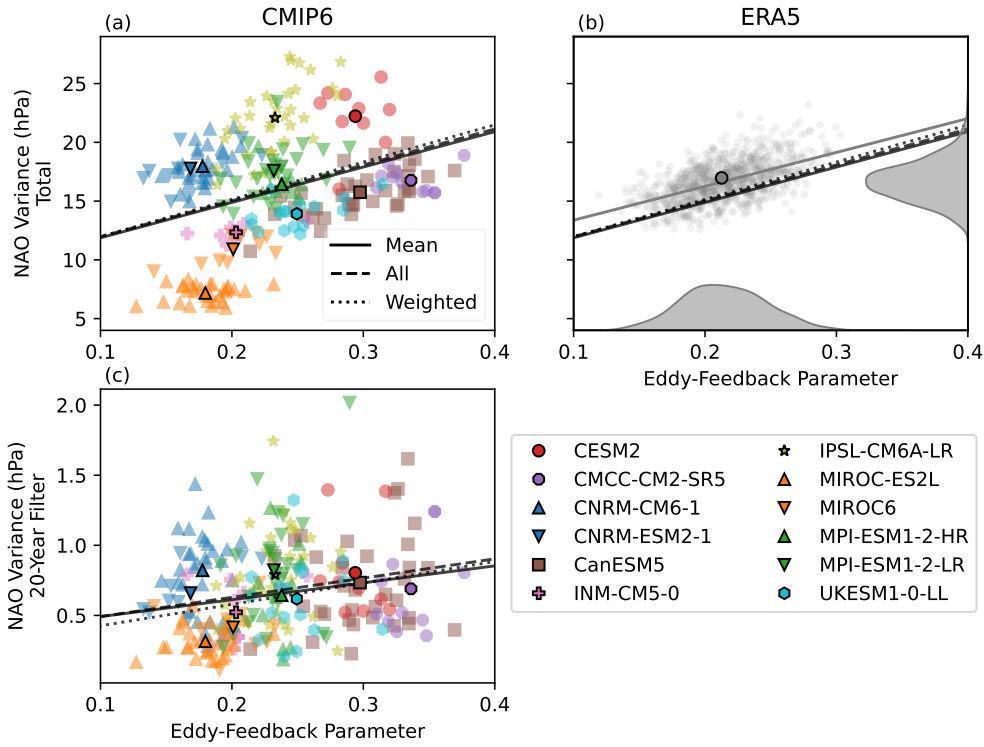


Figure 3. The relationship between the EFP and NAO variance for (a, c) CMIP6 historical simulations (1850-2014) and (b) ERA5 (full period, 1940-2022). (a) The EFP and NAO variance for CMIP6 ensemble members and mean for each model ensemble (outlined symbols). (b) EFP and NAO variance calculated using 164 years sampled from ERA5 with replacement (repeated 1000 times). The outlined dot shows the EFP and NAO variance for the full ERA5 data. (c) The same as (a), but for NAO variance calculated after applying a 20-year running-mean filter. The lines on each subfigure show linear regressions calculated from each set of data in the subfigures (see text for details). The lines from (a) are duplicated in (b) for comparison.

293 show how sampling issues with the EFP can produce spurious relationships with the NAO
 294 rather than identifying significant relationships.

295 All three regressions in Figure 3a show a similar relationship between EFP and NAO
 296 variance and are well reproduced by sampling ERA5 ($r=0.34-0.55$). This means that the
 297 across model relationship between the EFP and NAO variance (“Mean”), which could
 298 have been interpreted as physically related model biases, is most likely an extension of
 299 the sampling relationship found in ERA5: a model with stronger NAO variability is di-
 300 agnosed with a larger EFP.

301 Although total NAO variability is relatively well represented for models exhibiting
 302 the signal-to-noise paradox (Scaife & Smith, 2018), weak multidecadal NAO vari-
 303 ability Bracegirdle (2022); Bonnet et al. (2024) could be evidence of signal-to-noise is-
 304 sues in climate models. However, similar relationships are found when multidecadal vari-
 305 ability is isolated (Fig. 3c), suggesting this is still only identifying sampling relationships.
 306 We haven’t estimated the reanalysis relationship between the EFP and multidecadal NAO
 307 variance because ERA5 is too short for sampling and longer-timescale reanalyses give
 308 less consistent values of NAO further back in time (see supplement Figs. S3 and S4).

309 3.4 Alternative measure of eddy feedback

310 We next show that an alternative measure of eddy feedback targeted at the North
 311 Atlantic (G_{NA} , see section 2.2.2) suffers much less from the sampling issues identified
 312 for the EFP. Figure 4 shows G_{NA} for ERA5 and the CMIP6 ensembles and its relation-
 313 ship to NAO variance and the EFP. G_{NA} is better able to identify models that are weak
 314 (CanESM5, CESM2, IPSL-CM6A-LR, CMCC-CM2-SR5, INM-CM5-0, MIROC6, MIROC-
 315 ES2L), strong (MPI-ESM1-2-LR/HR), or unbiased (UKESM1-0-LL, CNRM-CM6-1, CNRM-
 316 ESM2-1) compared to ERA5 due to having much smaller sampling uncertainty.

317 The sampling relationship between G_{NA} and NAO variability in ERA5 is much weaker
 318 ($r=0.07$) in contrast to that of the EFP and NAO variability ($r=0.55$). Furthermore, the
 319 relationship differs from the (nonsignificant) across model relationship. Similar results
 320 are found for multidecadal NAO variability. Interestingly G_{NA} shows no sampling re-
 321 lationship to the EFP and very little relationship across the models used here (Fig 4d,e).
 322 This suggests that either the EFP is capturing different aspects of eddy feedback, due
 323 to G_{NA} being more localized, or that the EFP is a poor measure of eddy feedback due
 324 to the sampling issues shown in earlier.

325 4 Conclusions

326 Previous studies have suggested that seasonal prediction systems and free running
 327 climate models systematically underestimate Northern hemisphere midlatitude eddy feed-
 328 backs (Smith et al., 2022; Screen et al., 2022), and that this bias may explain the signal-
 329 to-noise paradox (Scaife et al., 2019; Hardiman et al., 2022). However, we find that the
 330 eddy feedback parameter (EFP) used by Smith et al. (2022), Screen et al. (2022), and
 331 Hardiman et al. (2022) exhibits large sampling uncertainty which can impede model-reanalysis
 332 comparisons and makes determining physical mechanisms difficult.

333 We have shown that the EFP is sensitive to individual outlier seasons and also ex-
 334 hibits strong multidecadal variability. This makes the EFP problematic to interpret as
 335 an intrinsic property of a model or the real world because very large sample sizes are needed
 336 to produce an estimate with sufficiently small uncertainties. Previous published estimates
 337 of the EFP in modern reanalysis data are close to the maximum value derived within
 338 the 1940-2022 period because of the pronounced effect of an outlier season (2009/10) and
 339 the phasing of multidecadal variability in the EFP. When sampling uncertainty is taken
 340 into account, the EFP in CMIP6 historical simulations is largely consistent with ERA5.

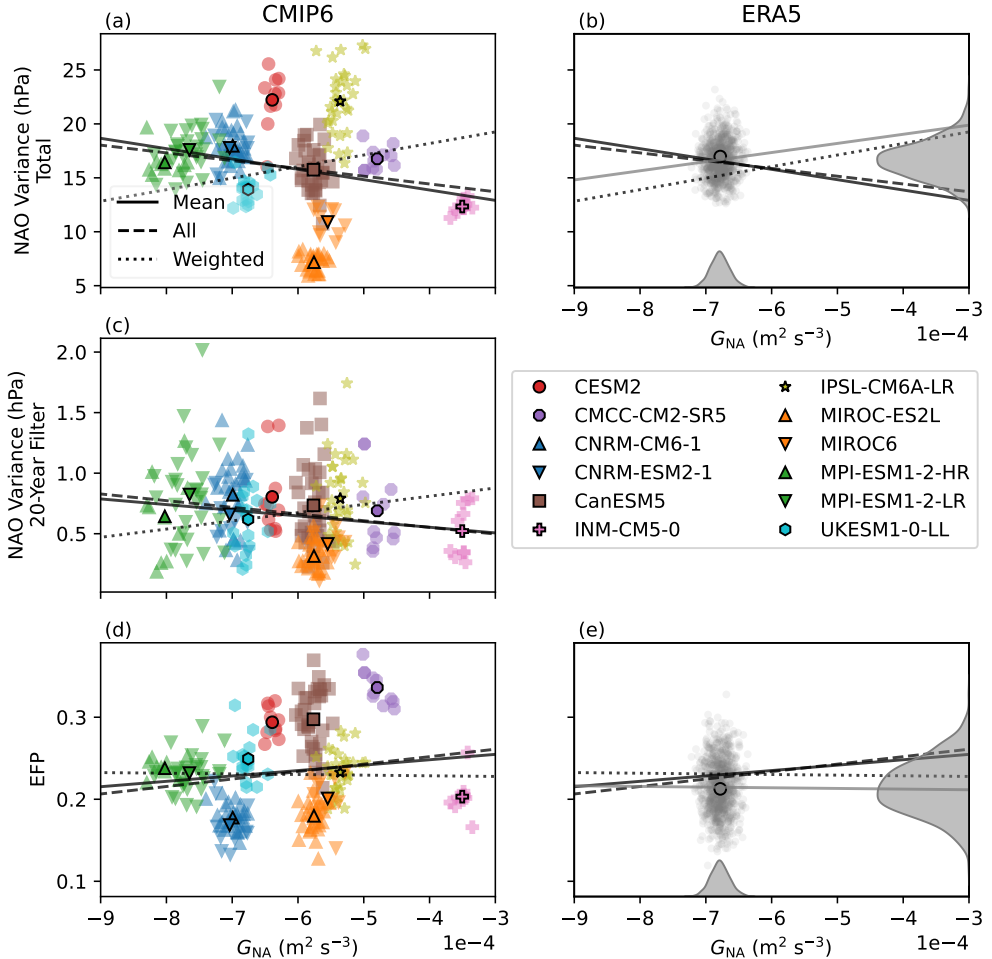


Figure 4. The same as Fig. 3, but with North-Atlantic DJF-mean barotropic energy generation rate (G_{NA}) on the x-axis instead of EFP and extra panels (d) and (e) with EFP on the y-axis for CMIP6 models and ERA5, respectively.

341 Previous results using the EFP as an emergent constraint (Smith et al., 2022; Screen et
 342 al., 2022) should have much larger error bars to account for these sampling uncertainties.
 343 These uncertainties may be the reason that Screen et al. (2022) found that the re-
 344 analysis EFP in the Southern Hemisphere is roughly in the middle of the model values,
 345 while the Northern Hemisphere EFP appeared too weak in models.

346 We have also shown that the sample EFP correlates with sample NAO variability
 347 and this can lead to spurious across-model correlations between the EFP and NAO vari-
 348 ability. The across model correlation could have been interpreted as a stronger model
 349 eddy feedback causing stronger NAO variability, but is actually due to a sample with
 350 stronger NAO variability being diagnosed with a stronger EFP because the EFP and NAO
 351 are not independent. The relation between the EFP and NAO makes sense because both
 352 variables have an underlying relationship with jet latitude. For example, winter 2009/10
 353 had an anomalously southward shifted jet and negative NAO (Santos et al., 2013) and
 354 makes the largest single contribution to the EFP in ERA5. It could be argued that mod-
 355 els with stronger eddy feedbacks would produce more years like 2009/10; however, it is
 356 clear that we need a much larger sample of data than is available for reanalyses to de-
 357 termine if this is the case.

358 We have investigated another measure of eddy feedback, the barotropic energy gen-
 359 eration rate G , which more cleanly separates eddy forcing and mean flow terms and can
 360 be calculated locally for the North Atlantic region (G_{NA}). G_{NA} shows much smaller sam-
 361 pling uncertainty than the EFP and a much weaker sampling relationship with NAO vari-
 362 ability, suggesting that it is better at describing intrinsic properties of the models and
 363 reanalysis. We find no systematic bias in G_{NA} , but G_{NA} does better distinguish which
 364 models are too weak, too strong or unbiased.

365 In summary, our results raise questions about previous interpretations that weak
 366 eddy feedbacks can explain the signal-to-noise paradox. Firstly, we find that models do
 367 not systematically underestimate eddy feedbacks when accounting for sampling uncer-
 368 tainty in the EFP or using an alternative, better constrained, diagnostic (G_{NA}). Secondly,
 369 the diagnosed EFP from a sample is dependent on the sample NAO variability, which
 370 makes it difficult to interpret differences associated with the EFP as being caused by eddy
 371 feedbacks rather than some confounding variable. Therefore previous results should be
 372 re-examined with a diagnostic of eddy feedback that is more robust to climate variabil-
 373 ity and where clearer causality can be determined, such as the barotropic energy gen-
 374 eration rate or a more in depth lead-lag approach that formally isolates the feedback of
 375 eddies on the mean flow (e.g., Lorenz and Hartmann (2001)).

376 Data availability

377 The ERA5 reanalysis data is available from the Copernicus Climate Data Store.
 378 ERA20C was accessed from the NCAR research data archive. The CMIP6 data used in
 379 the study was accessed from the Earth System Grid Federation. The diagnostics calcu-
 380 lated for each CMIP6 simulation are given in the supplement (Table S6). The code used
 381 for calculating the diagnostics is available at github.com/leosaffin/constrain and
 382 the code for further processing and making the figures is available at github.com/leosaffin/
 383 [eddy_feedback](https://github.com/leosaffin/eddy_feedback).

384 Acknowledgments

385 We gratefully acknowledge funding for this work by the EU Horizon 2020 project CON-
 386 STRAIN (GA no. 820829). We are grateful to Doug Smith and Steven Hardiman for con-
 387 structive discussion about the work.

388 **References**

- 389 Allan, R., & Ansell, T. (2006). A New Globally Complete Monthly Historical Grid-
 390 ded Mean Sea Level Pressure Dataset (HadSLP2): 1850–2004. *Journal of Cli-
 391 mate*, 19(22), 5816–5842. Retrieved from <https://journals.ametsoc.org/view/journals/clim/19/22/jcli3937.1.xml> doi: <https://doi.org/10.1175/JCLI3937.1>
- 394 Andrews, M. B., Knight, J. R., Scaife, A. A., Lu, Y., Wu, T., Gray, L. J., & Schen-
 395 zinger, V. (2019). Observed and simulated teleconnections between the strato-
 396 spheric quasi-biennial oscillation and northern hemisphere winter atmospheric
 397 circulation. *Journal of Geophysical Research: Atmospheres*, 124(3), 1219–
 398 1232. Retrieved from <https://agupubs.onlinelibrary.wiley.com/doi/abs/10.1029/2018JD029368> doi: <https://doi.org/10.1029/2018JD029368>
- 400 Beffort, D. J., Wild, S., Kruschke, T., Ulbrich, U., & Leckebusch, G. C. (2016,
 401 nov). Different long-term trends of extra-tropical cyclones and windstorms
 402 in ERA-20C and NOAA-20CR reanalyses. *Atmospheric Science Letters*,
 403 17(11), 586–595. Retrieved from <https://doi.org/10.1002/asl.694> doi:
 404 <https://doi.org/10.1002/asl.694>
- 405 Bloomfield, H. C., Shaffrey, L. C., Hodges, K. I., & Vidale, P. L. (2018). A critical
 406 assessment of the long-term changes in the wintertime surface Arctic Oscilla-
 407 tion and Northern Hemisphere storminess in the ERA20C reanalysis. *Environ-
 408 mental Research Letters*, 13(9), 94004. Retrieved from <https://dx.doi.org/10.1088/1748-9326/aad5c5> doi: 10.1088/1748-9326/aad5c5
- 410 Bonnet, R., McKenna, C., & Maycock, A. (2024, jan). Model spread in multidecadal
 411 NAO variability connected to stratosphere-troposphere coupling. *EGU-
 412 sphere*, 2024, 1–24. Retrieved from <https://egusphere.copernicus.org/preprints/2024/egusphere-2023-3103/>
 413 <https://egusphere.copernicus.org/preprints/2024/egusphere-2023-3103/egusphere-2023-3103.pdf>
 414 doi: 10.5194/egusphere-2023-3103
- 416 Bracegirdle, T. J. (2022, jun). Early-to-Late Winter 20th Century North At-
 417 lantic Multidecadal Atmospheric Variability in Observations, CMIP5 and
 418 CMIP6. *Geophysical Research Letters*, 49(11), e2022GL098212. Retrieved from
 419 <https://doi.org/10.1029/2022GL098212> doi: <https://doi.org/10.1029/2022GL098212>
- 421 Bracegirdle, T. J., Lu, H., Eade, R., & Woollings, T. (2018, jul). Do CMIP5 Models
 422 Reproduce Observed Low-Frequency North Atlantic Jet Variability? *Geophys-
 423 ical Research Letters*, 45(14), 7204–7212. Retrieved from <https://doi.org/10.1029/2018GL078965>
 424 <https://onlinelibrary.wiley.com/doi/10.1029/2018GL078965> doi: 10.1029/2018GL078965
- 426 Eade, R., Smith, D., Scaife, A., Wallace, E., Dunstone, N., Hermanson, L., & Robin-
 427 son, N. (2014). Do seasonal-to-decadal climate predictions underestimate
 428 the predictability of the real world? *Geophysical Research Letters*, 41(15),
 429 5620–5628. Retrieved from <https://doi.org/10.1002/2014GL061146> doi:
 430 <https://doi.org/10.1002/2014GL061146>
- 431 Eyring, V., Bony, S., Meehl, G. A., Senior, C. A., Stevens, B., Stouffer, R. J., &
 432 Taylor, K. E. (2016, may). Overview of the Coupled Model Intercompari-
 433 son Project Phase 6 (CMIP6) experimental design and organization. *Geosci.
 434 Model Dev.*, 9(5), 1937–1958. Retrieved from <https://gmd.copernicus.org/articles/9/1937/2016/>
 435 <https://gmd.copernicus.org/articles/9/1937/2016/gmd-9-1937-2016.pdf> doi: 10.5194/gmd-9-1937-2016
- 437 Fukotomi, Y., & Yasunari, T. (2002). Tropical-Extratropical Interaction Associated
 438 with the 10–25-day Oscillation over the Western Pacific during the Northern
 439 Summer. *Journal of the Meteorological Society of Japan. Ser. II*, 80(2), 311–
 440 331. Retrieved from http://www.jstage.jst.go.jp/article/jmsj/80/2/80_2_311/_article doi: 10.2151/jmsj.80.311
- 442 Gray, L. J., Scaife, A. A., Mitchell, D. M., Osprey, S., Ineson, S., Hardiman, S.,

- 443 ... Kodera, K. (2013, dec). A lagged response to the 11 year solar cycle
 444 in observed winter Atlantic/European weather patterns. *Journal of Geo-*
 445 *physical Research: Atmospheres*, 118(24), 13,405–413,420. Retrieved from
 446 <https://doi.org/10.1002/2013JD020062> doi: <https://doi.org/10.1002/2013JD020062>
- 447 Hardiman, S. C., Dunstone, N. J., Scaife, A. A., Smith, D. M., Comer, R., Nie,
 448 Y., & Ren, H.-L. (2022). Missing eddy feedback may explain weak signal-
 449 to-noise ratios in climate predictions. *npj Clim. Atmos. Sci.*, 5(1), 57.
 450 Retrieved from <https://doi.org/10.1038/s41612-022-00280-4> doi:
 451 [10.1038/s41612-022-00280-4](https://doi.org/10.1038/s41612-022-00280-4)
- 452 Hersbach, H., Bell, B., Berrisford, P., Hirahara, S., Horányi, A., Muñoz-Sabater, J.,
 453 ... Thépaut, J.-N. (2020). The ERA5 global reanalysis. *Q. J. R. Meteorol. Soc.*, 146(730), 1999–2049. Retrieved from <https://doi.org/10.1002/qj.3803> doi: <https://doi.org/10.1002/qj.3803>
- 454 Krueger, O., Schenk, F., Feser, F., & Weisse, R. (2013). Inconsistencies between
 455 Long-Term Trends in Storminess Derived from the 20CR Reanalysis and Ob-
 456 servations. *Journal of Climate*, 26(3), 868–874. Retrieved from <https://journals.ametsoc.org/view/journals/clim/26/3/jcli-d-12-00309.1.xml>
 457 doi: <https://doi.org/10.1175/JCLI-D-12-00309.1>
- 458 Lorenz, D. J., & Hartmann, D. L. (2001). Eddy-Zonal Flow Feedback in the South-
 459 ern Hemisphere. *Journal of the Atmospheric Sciences*, 58(21), 3312–3327.
 460 Retrieved from https://journals.ametsoc.org/view/journals/atsc/58/21/1520-0469{_}2001{_}058{_}3312{_}ezffit{_}2.0.co{_}2.xml
 461 doi: [https://doi.org/10.1175/1520-0469\(2001\)058<3312:EZFFIT>2.0.CO;2](https://doi.org/10.1175/1520-0469(2001)058<3312:EZFFIT>2.0.CO;2)
- 462 Lorenz, D. J., & Hartmann, D. L. (2003). Eddy-Zonal Flow Feedback in the
 463 Northern Hemisphere Winter. *Journal of Climate*, 16(8), 1212–1227. Re-
 464 tried from https://journals.ametsoc.org/view/journals/clim/16/8/1520-0442_2003_16_1212_effitn_2.0.co_2.xml doi: [https://doi.org/10.1175/1520-0442\(2003\)16<1212:EFFITN>2.0.CO;2](https://doi.org/10.1175/1520-0442(2003)16<1212:EFFITN>2.0.CO;2)
- 465 Luo, D., Gong, T., & Diao, Y. (2007). Dynamics of eddy-driven low-frequency dipole
 466 modes. part iii: Meridional displacement of westerly jet anomalies during two
 467 phases of nao. *Journal of the Atmospheric Sciences*, 64(9), 3232 - 3248. Re-
 468 tried from <https://journals.ametsoc.org/view/journals/atsc/64/9/jas3998.1.xml> doi: <https://doi.org/10.1175/JAS3998.1>
- 469 Mak, M., & Cai, M. (1989). Local Barotropic Instability. *J. Atmos. Sci.*, 46(21),
 470 3289–3311. Retrieved from https://journals.ametsoc.org/view/journals/atsc/46/21/1520-0469{_}1989{_}046{_}3289{_}1bi{_}2{_}0{_}co{_}2.xml
 471 doi: [https://doi.org/10.1175/1520-0469\(1989\)046<3289:LBI>2.0.CO;2](https://doi.org/10.1175/1520-0469(1989)046<3289:LBI>2.0.CO;2)
- 472 McKenna, C. M., & Maycock, A. C. (2021). Sources of uncertainty in multimodel
 473 large ensemble projections of the winter north atlantic oscillation. *Geophys-
 474 ical Research Letters*, 48(14), e2021GL093258. Retrieved from <https://agupubs.onlinelibrary.wiley.com/doi/abs/10.1029/2021GL093258>
 475 (e2021GL093258 2021GL093258) doi: <https://doi.org/10.1029/2021GL093258>
- 476 Oliver, E. C. J. (2016, aug). Blind use of reanalysis data: apparent trends in Mad-
 477 den–Julian Oscillation activity driven by observational changes. *International
 478 Journal of Climatology*, 36(10), 3458–3468. Retrieved from <https://doi.org/10.1002/joc.4568>
 479 doi: <https://doi.org/10.1002/joc.4568>
- 480 O'Reilly, C. H., Weisheimer, A., Woollings, T., Gray, L. J., & MacLeod, D. (2019,
 481 jan). The importance of stratospheric initial conditions for winter North
 482 Atlantic Oscillation predictability and implications for the signal-to-noise
 483 paradox. *Q. J. R. Meteorol. Soc.*, 145(718), 131–146. Retrieved from
 484 <https://doi.org/10.1002/qj.3413> doi: <https://doi.org/10.1002/qj.3413>
- 485 Ossó, A., Sutton, R., Shaffrey, L., & Dong, B. (2020). Development, Amplification,
 486 and Decay of Atlantic/European Summer Weather Patterns Linked to Spring
 487

- 498 North Atlantic Sea Surface Temperatures. *J. Clim.*, 33(14), 5939–5951. Retrieved from <https://journals.ametsoc.org/view/journals/clim/33/14/JCLI-D-19-0613.1.xml> doi: <https://doi.org/10.1175/JCLI-D-19-0613.1>
- 499 Parker, T., Woollings, T., Weisheimer, A., O'Reilly, C., Baker, L., & Shaffrey, L.
500 (2019, aug). Seasonal Predictability of the Winter North Atlantic Oscillation From a Jet Stream Perspective. *Geophys. Res. Lett.*, 46(16), 10159–
501 10167. Retrieved from <https://doi.org/10.1029/2019GL084402> doi:
502 <https://doi.org/10.1029/2019GL084402>
- 503 Poli, P., Hersbach, H., Dee, D. P., Berrisford, P., Simmons, A. J., Vitart, F., ...
504 Fisher, M. (2016). ERA-20C: An Atmospheric Reanalysis of the Twentieth
505 Century. *Journal of Climate*, 29(11), 4083–4097. Retrieved from <https://journals.ametsoc.org/view/journals/clim/29/11/jcli-d-15-0556.1.xml>
506 doi: <https://doi.org/10.1175/JCLI-D-15-0556.1>
- 507 Santos, J. A., Woollings, T., & Pinto, J. G. (2013). Are the Winters 2010 and
508 2012 Archetypes Exhibiting Extreme Opposite Behavior of the North At-
509 lantic Jet Stream? *Mon. Weather Rev.*, 141(10), 3626–3640. Retrieved
510 from <https://journals.ametsoc.org/view/journals/mwre/141/10/mwr-d-13-00024.1.xml> doi: <https://doi.org/10.1175/MWR-D-13-00024.1>
- 511 Scaife, A. A., Arribas, A., Blockley, E., Brookshaw, A., Clark, R. T., Dunstone,
512 N., ... Williams, A. (2014). Skillful long-range prediction of Euro-
513 pean and North American winters. *Geophys. Res. Lett.*, 41(7), 2514–
514 2519. Retrieved from <https://doi.org/10.1002/2014GL059637> doi:
515 <https://doi.org/10.1002/2014GL059637>
- 516 Scaife, A. A., Camp, J., Comer, R., Davis, P., Dunstone, N., Gordon, M., ... Vi-
517 dale, P. L. (2019). Does increased atmospheric resolution improve seasonal
518 climate predictions? *Atmospheric Science Letters*, 20(8), e922. Retrieved from
519 <https://rmets.onlinelibrary.wiley.com/doi/abs/10.1002/asl.922> doi:
520 <https://doi.org/10.1002/asl.922>
- 521 Scaife, A. A., & Smith, D. (2018). A signal-to-noise paradox in climate science.
522 *npj Clim. Atmos. Sci.*, 1(1), 28. Retrieved from <https://doi.org/10.1038/s41612-018-0038-4> doi: 10.1038/s41612-018-0038-4
- 523 Screen, J. A., Eade, R., Smith, D. M., Thomson, S., & Yu, H. (2022, dec). Net
524 Equatorward Shift of the Jet Streams When the Contribution From Sea-Ice
525 Loss Is Constrained by Observed Eddy Feedback. *Geophys. Res. Lett.*, 49(23),
526 e2022GL100523. Retrieved from <https://doi.org/10.1029/2022GL100523>
527 doi: <https://doi.org/10.1029/2022GL100523>
- 528 Simpson, I. R., Deser, C., McKinnon, K. A., & Barnes, E. A. (2018). Modeled and
529 Observed Multidecadal Variability in the North Atlantic Jet Stream and Its
530 Connection to Sea Surface Temperatures. *Journal of Climate*, 31(20), 8313–
531 8338. Retrieved from <https://journals.ametsoc.org/view/journals/clim/31/20/jcli-d-18-0168.1.xml> doi: 10.1175/JCLI-D-18-0168.1
- 532 Slivinski, L. C., Compo, G. P., Whitaker, J. S., Sardeshmukh, P. D., Giese, B. S.,
533 McColl, C., ... Wyszyński, P. (2019, oct). Towards a more reliable his-
534 torical reanalysis: Improvements for version 3 of the Twentieth Century
535 Reanalysis system. *Quarterly Journal of the Royal Meteorological Society*,
536 145(724), 2876–2908. Retrieved from <https://doi.org/10.1002/qj.3598>
537 doi: <https://doi.org/10.1002/qj.3598>
- 538 Smith, D. M., Eade, R., Andrews, M. B., Ayres, H., Clark, A., Chripko, S., ...
539 Walsh, A. (2022). Robust but weak winter atmospheric circulation re-
540 sponse to future Arctic sea ice loss. *Nat. Commun.*, 13(1), 727. Retrieved
541 from <https://doi.org/10.1038/s41467-022-28283-y> doi:
542 10.1038/s41467-022-28283-y
- 543 Smith, D. M., Eade, R., Scaife, A. A., Caron, L.-P., Danabasoglu, G., DelSole,
544 T. M., ... Yang, X. (2019). Robust skill of decadal climate predictions. *npj
545 Clim. Atmos. Sci.*, 2(1), 13. Retrieved from <https://doi.org/10.1038/s41612-018-0038-4>
- 546

- 553 s41612-019-0071-y <https://www.nature.com/articles/s41612-019-0071-y>
554 doi: 10.1038/s41612-019-0071-y
- 555 Stephenson, D. B., Pavan, V., Collins, M., Junge, M. M., Quadrelli, R., & Groups,
556 P. C. M. (2006). North Atlantic Oscillation response to transient greenhouse
557 gas forcing and the impact on European winter climate: a CMIP2 multi-model
558 assessment. *Climate Dynamics*, 27(4), 401–420. Retrieved from <https://doi.org/10.1007/s00382-006-0140-x> doi: 10.1007/s00382-006-0140-x
- 560 Strommen, K. (2020, jul). Jet latitude regimes and the predictability of the North
561 Atlantic Oscillation. *Quarterly Journal of the Royal Meteorological Society*,
562 146(730), 2368–2391. Retrieved from <https://doi.org/10.1002/qj.3796>
563 doi: <https://doi.org/10.1002/qj.3796>
- 564 Williams, N. C., Scaife, A. A., & Screen, J. A. (2023, mar). Underpredicted ENSO
565 Teleconnections in Seasonal Forecasts. *Geophysical Research Letters*, 50(5),
566 e2022GL101689. Retrieved from <https://doi.org/10.1029/2022GL101689>
567 doi: <https://doi.org/10.1029/2022GL101689>
- 568 Woollings, T., Hannachi, A., & Hoskins, B. (2010, apr). Variability of the North
569 Atlantic eddy-driven jet stream. *Quarterly Journal of the Royal Meteorological
570 Society*, 136(649), 856–868. doi: 10.1002/qj.625